

## On the properties and resistance to abrasive wear of surface-modified Ti6Al4V alloy by laser shock processing

Chávez J.<sup>1</sup>, Rodríguez E., Flores M., Ibarra-Montalvo J., Jiménez O.  
 Departamento de Ingeniería de Proyectos, Universidad de Guadalajara  
 José Guadalupe Zuno # 48, Los Belenes, Zapopan, Jalisco, C.P. 45100, México

Gómez-Rosas G.  
 Departamento de Física Centro Universitario de Ciencias Exactas e Ingenierías  
 Universidad de Guadalajara. Guadalajara Jalisco, México  
 (Recibido: 5 de enero de 2013; Aceptado: 30 de abril de 2014)

The application of traditional surface modification techniques to improve mechanical properties of a wide range of materials has been used for at least three decades with important results. More recently, newer and innovative techniques such as Laser Shock Processing (LSP) have gained popularity due to the benefits offered. In this work, Ti6Al4V alloy was treated under several conditions of laser density and wavelength during the treatment. The roughness of the samples before and after treatment was measured by profilometry. The resultant surface roughness average ( $R_a$ ) is in the range for biomedical implants. The microhardness values were taken from the sample cross-section showing no increment after being treated with LSP. X-ray diffraction (XRD) was used for phase identification and possible changes in the lattice parameters. The abrasive wear resistance was evaluated by means of ball cratering tests, the wear volume was assessed measuring wear scars using profilometry from which the wear rate was calculated. Samples treated with LSP were in some cases more susceptible to abrasive wear than the untreated material.

*Keywords:* Ball cratering; LSP; Hardness; Structure

### 1. Introduction

Titanium alloys are one of the selected materials for certain applications such as aerospace, medical and industrial, especially where properties such as low density, high corrosion resistance and good biocompatibility are needed. Titanium alloys have also significant disadvantages such as low hardness and poor resistance to wear and fatigue [1, 2]. Over the past three decades there have been studies on this material trying to improve its faults. Coatings and surface treatments have been used; although they are not completely effective for some specific applications. Therefore, alternative routes of surface treatment are taken into account such is the case of Laser Shock Processing (LSP)[3]. The LSP is a process that can generate several effects in metallic materials, using a high energy laser. The aim of this treatment is the generation of residual compressive stresses in the surface of the material by means of induction of cold work that is produced by the impact of a laser beam in a certain area [3]. This method has the advantage of inducing residual stress up to a depth of ~1 mm in the material as it has been demonstrated in the work of M. Rozmus[4]. Another advantage of LSP treatment is its ability to increase the hardness of a variety of materials up to 10% near the surface [5]. In Ti6Al4V, microhardness increased by 15% with a single impact and 24% with two consecutive impacts in the same area [5]. A schematic of the LSP treatment principle is shown in Figure 1. When a laser beam hits the surface material with a sufficiently high density laser pulse, shock waves or pressure waves are generated. If the peak pressure of these waves is greater

than the yield strength of the material, the surface can be plastically deformed and can be induced compressive residual stresses. This causes an increment in the resistance of the material surface in terms of fracture and failure fatigue [3, 6]. When a material is irradiated with power densities greater than  $10^8 \text{ W}\cdot\text{cm}^{-2}$ , the shock wave formed may induce residual stresses to the material which may change the mechanical and tribological properties of the surface of the material. The properties prone to be changed are among others, hardness, yield strength and wear resistance [7, 8]. Another benefit of LSP treatment is the resultant surface roughness which depends on the parameters and the material. This treatment has then, the potential for certain biomedical applications such as implants which require roughness between 1.5 and 4  $\mu\text{m}$  [9, 10]. This roughness range allows an efficient contact between the implant and the bone and it is said that the response of bone to the implant is influenced by the topography of the implant [11]. In this work we study the Ti6Al4V alloy, with and without LSP treatment in terms of its mechanical and tribological properties, the effect of some treatment parameters on these properties is also explored.

### 2. Experimental Procedure

Ti6Al4V circular coupons with a diameter of 30 mm and 5 mm thick were cut and grinded to achieve uniformity in roughness of ~200 nm before the treatment. LSP was performed using a laser Brilliant b Quantel having an active medium of laser beam generation Nd: YAG, providing a maximum pulse energy of 1 J with a

**Table 1.** Parameters used in the radiation of samples.

RADIATION PARAMETERS					
Sample	Laser energy measured (J)	Pulse (cm <sup>2</sup> )	Wavelength (nm)	Power density (GW/cm <sup>2</sup> )	Spot Diameter (mm)
S1a	0.44	5000	532	11.2	1
S1b	0.44	2500	532	11.2	1
S2a	0.88	5000	1064	8.2	1.5
S2b	0.88	2500	1064	8.2	1.5

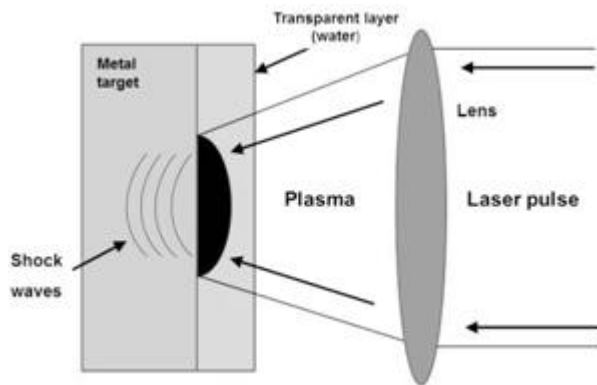


**Figure 1.** Schematic of the process of LSP.

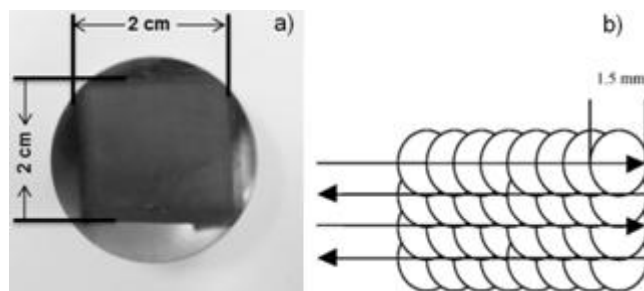


**Figure 2.** Treatment area with LSP a) and, sequence and direction of treatment showing overlapping and size of laser impacts b).

wavelength of 1064 nm and 0.5 J with a wavelength of 532 nm. The LSP treatment was conducted in confined environment and atmospheric air. The used parameters are shown in Table 1. Samples are divided into two groups according to the wavelength and density of the treatment. Samples were treated as shown with overlapping impact spots in an area of 4 cm<sup>2</sup>, Figure 2.

Surface roughness was performed using a profilometer Veeco Dektak 150. Cross sectional scans were made in order to determine the value of R<sub>a</sub> (average Roughness). At least five measurements from each sample were taken to register the statistical difference of results. Vickers hardness was measured as a function of depth from the surface of each specimen by means of a Future Tech FM-800 microhardness tester. Indentations were performed every 200 microns from the surface with a load of 100 gf and a dwell time of 20 s. X-ray Diffraction was used to identify phases in the material. Also, a process of polishing with 1 μm alumina was done in order to remove superficial residual material from treatment and to identify the phases at the top layer. The tests were conducted on a Siemens D500 diffractometer with a copper radiation of λ=0.154 nm. Scans were made from 30 to 80 degrees for the value of 2θ, at an angular velocity of 0.02 °/s, using a voltage of 20 kV and a current of 30 mA. In order to observe a possible shift of the main diffraction peak and associate this with the cell deformation and strain, fine scans were conducted using a 2θ range from 39.5 to 41.5 using a scan rate of 0.01 °/s, with the other parameters kept constant. The wear resistance was measured through ball cratering test, which is a technique that generates microabrasion through a steel sphere of known radius that is continuously wetted with a liquid abrasive (a slurry). The test produces a wear scar and the volume of displaced material is calculated using the following formula:

$$V = \frac{1}{3} \pi h^2 (3R - h) \tag{1}$$

$$V = \frac{\pi b^4}{64R} \text{ for } b \ll R \tag{2}$$

where *b* is the diameter of the crater and *R* the radius of the sphere. This relationship assumes that the shape of the crater is dependent on the shape of the sphere [12-15]. The

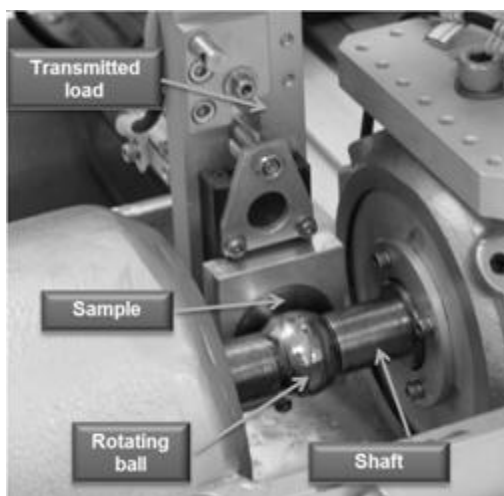


**Figure 3.** Microabrasion equipment for ball cratering wear test.

wear law from Archard [16, 17] states that the amount of wear is determined by:

$$V = KsN \quad (3)$$

where  $K$  is a wear rate constant,  $s$  is the distance of sliding and  $N$  is the load applied to the sample [14, 16]. Constant wear rate is then calculated as follows [14, 16]:

$$K = \frac{\pi b^4}{64RSN} \quad (4)$$

It was established that the severity of contact  $S$  can be obtained by equation [18]:

$$S = \frac{W}{AvH'} \quad (5)$$

where  $W$  is the load applied between the sphere and the sample,  $A$  is the area of the wear scar or interaction area which is defined by equation (6),  $v$  is the volume fraction of the abrasive slurry.

$$A = \pi a'^2 = \pi (a^2 + 2Rd) \quad (6)$$

$$a = \frac{1}{2/R} \quad (7)$$

$H'$  is the hardness effective which is given by equation (8) [18].

$$\frac{1}{H'} = \frac{1}{H_e} + \frac{1}{H_m} \quad (8)$$

where  $a$  is the radius of the Hertzian contact area,  $R$  is the ball radius and  $d$  is the diameter of the abrasive particles,  $H_e$  is the hardness of the ball and  $H_m$  is the hardness of the sample [18].

It has been found that one can define a critical severity Contact  $S^*$ , which empirically relates the hardness ratio  $H_m/H_b$  by [18]:

$$S^* = \alpha \left( \frac{H_m}{H_b} \right)^\beta \quad (9)$$

where  $H_b$  and  $H_m$  are the hardness of the sample and the hardness of the sphere respectively, and  $\alpha$  and  $\beta$  are empirical constants with  $\alpha=0.0076$  and  $\beta=-0.049$  for analyzed data for different hardness reasons  $H_m/H_b$  from 0.05 to 10 [18].

For the microabrasion tests, the equipment shown in Figure 3 was used. The equipment consists of a pendulum system for holding the sample which has vertical and horizontal position controls also, a rotating shaft is used during the test to hold the sample. Control of tests was made using a digital system that counts the revolutions of the ball which allows to calculate the total displacement distance.

The counterpart used was a SAE 52100 steel sphere with 25.4 mm of diameter. A slurry made of 5 $\mu$ m alumina abrasive particles in distilled water at a volume fraction of 0.24 $\pm$  0.03 was used as the abrasive media. The slurry was

constantly dropped between the sphere and the sample to maintain the sample wet during the test. The parameters used are shown in Table 2.

### 3. Results and Discussion

Surface roughness measurements showed that due to LSP treatment, roughness increased significantly with respect to the untreated sample. The average roughness ( $R_a$ ) of the samples increased from ~200 nm before treatment to >6500 nm after LSP. Figure 4 shows the variation of roughness between samples.

Looking at the treated samples, it can be observed that treatment with a wavelength of 532 nm generated higher surface roughness in comparison to those treated with a wavelength of 1064 nm. Also, a greater pulse density generated higher roughness. Such behavior of surface roughness variations is attributed to the power density selected for this investigation. It can be noted that the samples S1b, S2a and S2b final roughness is in the acceptable range considered in biomedical implants [9, 10], since bone area which is in contact with the surface of the implant is dependent on the roughness of the implant. It is well known that this difference of roughness affects the surface contact energy. In the investigation of A. Wennerberg [19] it was concluded that a surface with a roughness of ~1.4  $\mu$ m promotes better adhesion with the bone than a roughness of 1.2  $\mu$ m. The LSP treatment with the parameters used in this study can produce in a controlled way roughness in the range for using in biomedical applications. Figure 5 shows the microhardness profiles, due to the dispersion of the data these do not reveal any conclusive change in the value of the microhardness of the treated samples with respect to the untreated ones. The observed dispersion is attributed to the biphasic nature of the Ti6Al4V alloy due to the intrinsic properties of both phases  $\alpha$  and  $\beta$ . Dispersion of this type has also been reported in previous investigations where a

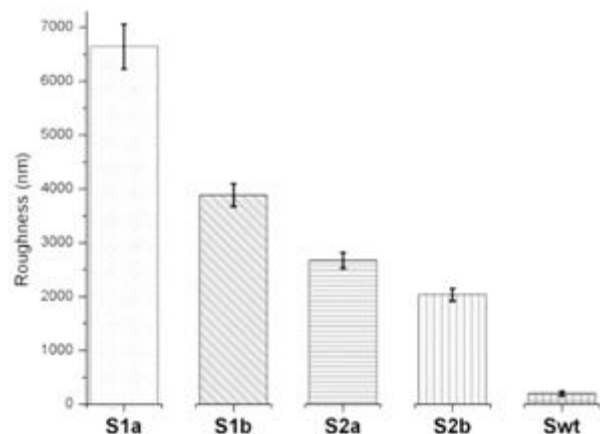


Figure 4. Roughness ( $R_a$ ) of samples treated with LSP.

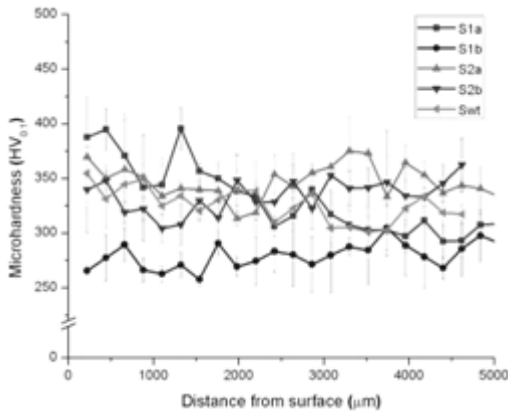


Figure 5. Vickers microhardness profiles of Ti6Al4V samples treated with LSP.

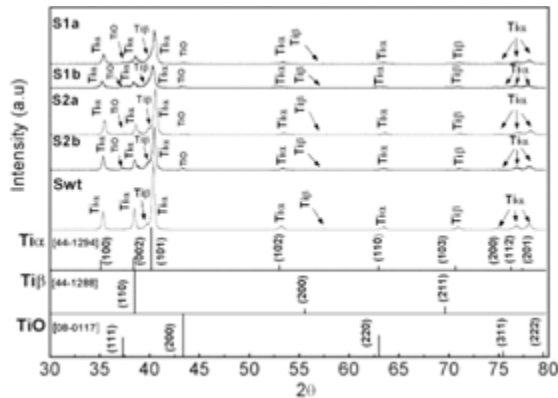


Figure 6. Diffraction patterns of Ti6Al4V samples with LSP processing.

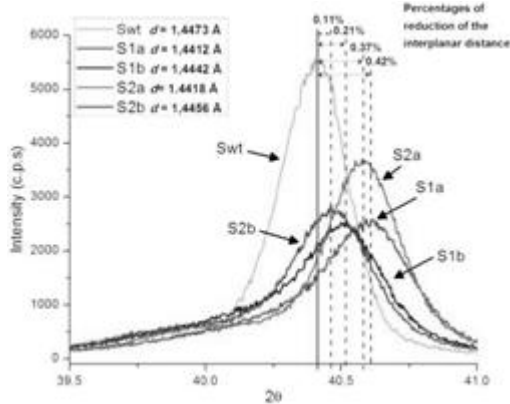


Figure 7. Shift of main peak ( $\alpha$  phase) of Ti.

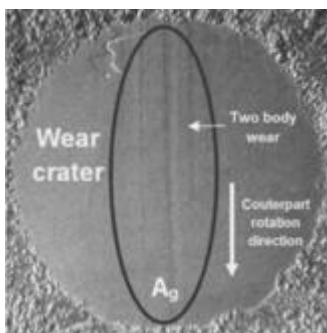


Figure 8. Crater of the sample S1b with a displacement of 200 m and 3 N, showing transition from two-body wear.

titanium alloy similar to that used in this work was studied [20]. The profiles on the graph do not show a trend involving an increment, therefore, it is not possible to attribute increased microhardness. This may be due to that a single impact does not generate hardening, unlike other investigations showed where an increment on the microhardness values was verified after LSP treatment [21, 22].

Figure 6 shows the X-ray diffraction patterns with the phases present in the alloy as well as the structural changes caused by LSP treatment. It was observed a clear shift for all  $\beta$  phase peaks approximately one degree with respect to the crystallographic reference card PDF 44-1288. This shift corresponds to a deformation of approximately 3% of the lattice of this phase ( $Ti\beta$ ), which is probably caused by the machining of the bar or the grinding process during preparation of the samples, as found in [23].

Diffraction patterns of the treated samples with LSP clearly show the appearance of two peaks at  $37.62^\circ$  and  $43.63^\circ$ ,  $2\theta$ , which do not correspond to the untreated material. These peaks were identified as  $TiO$  (111) and (200) from the PDF 08-0117 crystallographic database. The formation of titanium oxide is due to the interaction between the material surface and the water layer when the laser beam impacts the material. This oxide is formed only on the surface of the material and has been reported in other studies [3, 4, 24, 25]. It was observed that if the deformation layer is removed by a gentle polishing, the  $TiO$  peaks disappeared. Figure 7 shows a closer look at the main diffraction peak of the phase whose analysis was made between  $39.5^\circ$  and  $41^\circ$  of  $2\theta$ . The figure shows the shift in the main diffraction peak of the treated samples respect to untreated material in the (101) plane.

This shift to higher angles represents a decrement in the interplanar distance, which is attributed to mechanical deformation of the material caused by LSP although there are other reasons for this decrement in the lattice parameter such as phase transformation, thermal expansion, etc. [26]. It is also notable the reduction in the intensity of the diffraction peaks of the treated samples, which can be attributed to a slightly change in the orientation of the crystal lattice as a result of the treatment. This was also previously observed by L. Bengochea [27]. In this work, the minimum broadening of the diffraction peaks of the samples treated with LSP may explain a slight refinement of the particle size as similar observations were reported in [28].

In microabrasion tests, a thorough inspection of the craters with a stereoscopic microscope was made for the analysis of the abrasion wear, images showed two body type wear in the craters for short distances (100 and 200 meters) and loads of 2 and 3 N. The designation of the type of wear is selected according to a criteria presented in the literature [29, 30], which is the fraction of the area that shows two body wear (projected area fraction with grooving abrasion,  $A_g$ ) with respect to the total area of the crater (total Projected area,  $A_p$ ). When the crater under examination is in the condition  $A_g/A_p=0$  it is said that pure

**Table 2.** Microabrasion test parameters.

Load (N)	Speed (rpm)	Ball diameter (cm)	Sliding distance (m)
1, 2, 3	175	2.54	100, 200, 500, 1000

three body wear occurred and, if it is  $0 < A_g/A_p < 1$ , it is said that there is mixed wear (transition wear type) while if  $A_g/A_p = 1$  is observed, it is said that there is pure two body wear [29]. Figure 8 shows a crater showing transition to two body type wear.

The two body wear can be attributed to the fact that in the conditions used for the wear test (loads of 2 and 3 N and displacement of 100 and 200 meters), the pressure was relatively high and it is more difficult for the abrasive particles to roll compared to low pressures. Therefore, the characteristic grooves of the two body wear are observed similarly to other studies where the ball cratering test was conducted on various materials and parameters [13, 29,31]. It has been observed that the pressure can be reduced due to an increment in the contact area during the test, which can be calculated with the equation that defines the pressure in the test [32]:

$$P = \frac{N}{A} \tag{10}$$

where P is the pressure on the sample during the test, N is the normal load and A is the area of the crater. Two body wear does not happen at the lowest normal load (1N), possibly because the load is not high enough to allow the movement of the abrasive particles during the test.

Figure 9 shows the representative micro-abrasion craters obtained from long displacement distances such as 1000 meters. Image clearly shows that the type of predominant wear correspond to three body wear since neither the scratching pattern nor the grooves characteristic of the two body wear were seen.

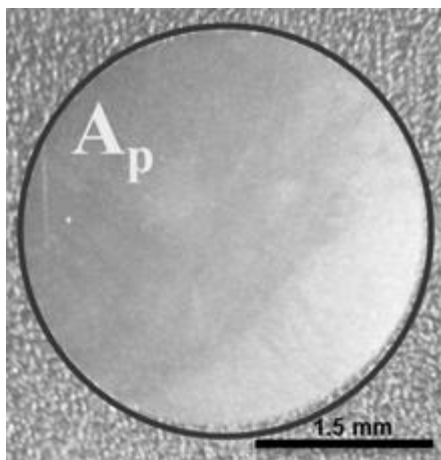


**Figure 9.** Crater of the sample S2b tested at 1 N and 1000 meter of displacement showing three body wear type.

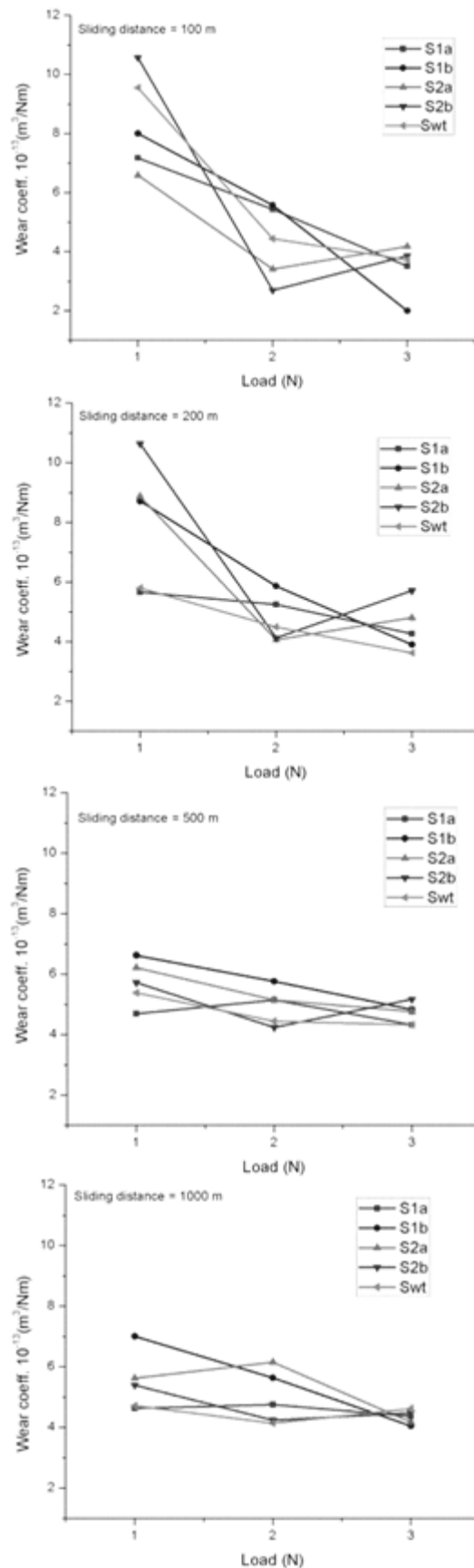


**Figure 10.** Graphs of wear coefficient vs load applied on ball cratering tests.

The reason for the three body type can be attributed to the fragmentation of abrasive particle after a long time of the test. After several revolutions in which the particle is rolling, this ends up breaking, reducing its size and changing its shape from angular to rounded, causing less severe wear (three body type). This phenomenon was seen in investigations of C. Cozza and M. Flores [18, 32]. Another possible cause of the presence of three body wear in the craters at long distances (500 and 1000 meters), is related to the pressure during the test, which is determinative on the type of wear. In this case, the contact area of the sphere increased, then, the pressure during the test was reduced considerably, which promoted the rolling of the abrasive particles to produce the three body type of wear predicted in other studies [18, 32]. Figure 10 shows the wear coefficient of treated samples with LSP and the untreated material with respect to the load applied during the test, the points on the graph are the average of three tests. The samples S1a, S1b and S2a showed lower wear coefficient than the untreated sample indicating that for low loads and short sliding distances the LSP treatment was effective in reducing the wear coefficient. The graphs indicate that when load increased, a decrement in the wear coefficient is observed. This can be explained by the equation (5); as the severity of contact decreases when the crater becomes larger (because the contact area increases). It is worth to mention that not all the lines have an evenly descending trend this is due to variation in the measurements obtained and, for the biphasic characteristic of the material. Another reason is that the abrasive behavior during testing i.e. as being independent particles, these suffer different type of deterioration [16, 33].

At low loads and short displacement distances increments on the value of the wear coefficient are most noticeable. This may be because the abrasive particles have not yet undergone any significant change in their size and/or original form. An abrasive particle of larger size and angular shaped usually is more aggressive in wear tests [16].

The graphs in figure 10 shows that the wear coefficient of treated samples with LSP have the same value approximately than the wear of untreated material, indicating that after LSP, samples show a tendency to wear similarly to untreated samples. This trend is more evident for the wear values at 500 and 1000 m. This may be attributed to the stress generated by the micro-abrasion machine, particularly to the generation of tangential stresses to the surface of the sphere. According to the literature, compressive residual stresses is generated perpendicular to the surface treated with LSP, results showed no benefit against abrasive wear measured by ball cratering, since the type of stress generated for this test is shear stress at the sample surface. From the results of the microabrasion wear test it can be stated that the LSP treatment (which would deliver compressive residual stress) did not show a clear trend to improve wear resistance. Then, the compressive residual stresses

generated may not be beneficial for ball cratering abrasive wear configurations [16].

#### 4. Conclusions

Samples with LSP treatment resulted with a final roughness greater than the samples without treatment. The range of roughness obtained was from 2.6 to 6.7  $\mu\text{m}$ . The final roughness could be suitable for applications in biomedical implants. Although LSP treatment is a good choice for hardening materials, in this research most of the samples treated showed no apparent change in the microhardness measured perpendicular to the treatment. A single laser impact does not generate measurable hardening. X-ray Diffraction showed the appearance of titanium oxide (TiO) at the surface of the treated samples. Also, a reduction in the interplanar distance of 0.42% was measured and, the intensity of the diffraction peaks caused by treatment distortion indicated induction of stresses in the material. Broadening of the peaks was also observed in treated samples suggesting a slight grain refinement, which shows that the material was affected by the treatment. Treated samples showed no tendency to increase the abrasive wear resistance in ball cratering tests, this fact is attributed to the incompatibility between the state of stress generated during the wear test and the stresses induced to the material by the LSP. We identified the transition in wear modes from two to three body which is consistent with the calculated contact severity.

#### References

- [1] M. Niinomi, Science and Technology of Advanced Materials **4**, 445(2003).
- [2] F. Torregrosa, L. Barrallier, L. Roux, Thin Solid Films **266**, 245(1995).
- [3] J.K. M. Rozmus, M. Blicharski, J. M., Archives of Metallurgy and Materials **54**, 665(2009).
- [4] M. Rozmus-Górnikowska, Acta Physica Polonica A **117**, 808(2010).
- [5] V.F. Niehoff Schulze H., Metallurgical **11**, 183(2005).
- [6] Y.W. Y. Fan, S. Vukelic, and Y.L. Yao, Journal of Applied Physics **98**, 104904(2005).
- [7] J.P. Chu, J.M. Rigsbee, G. Banaś, H.E. Elsayed-Ali, Materials Science and Engineering A **260**, 260(1999).
- [8] I.Y. Khalfallah, M.N. Rahoma, J.H. Abboud, K.Y. Benyounis, Optics & Laser Technology **43**, 806(2011).
- [9] E. Chikarakara, S. Naher, D. Brabazon, Appl. Phys. A **101**, 367(2010).
- [10] R.R. Iva Milinkovi, Karlo T. Rai, Zoran Aleks, Vojkan Lazi, Aleksandar Todorovi, Dragoslav Stamenkovi, MTAEC **946**, 251(2012).
- [11] M.M. Shalabi, A. Gortemaker, M.A.V.t. Hof, J.A. Jansen, N.H.J. Creugers, Journal of Dental Research **85**, 496(2006).
- [12] M.G. Gee, A. Gant, I. Hutchings, R. Bethke, K. Schiffman, K. Van Acker, S. Poulat, Y. Gachon, J. von Stebut, Wear **255**, 1(2003).
- [13] R.I. Trezona, D.N. Allsopp, I.M. Hutchings, Wear **225**, 205(1999).
- [14] C. Leroy, K.I. Schiffmann, K. van Acker, J. von Stebut, Surface and Coatings Technology **200**, 153(2005).

- [15] A.S.f. Metals, ASM handbook: Friction, lubrication, and wear technology, 1992.
- [16] I.M. Hutchings, Tribology. Friction and wear of engineering materials, (London, 2003).
- [17] G.W. Stachowiak, A.W. Batchelor, 8 - Boundary and Extreme Pressure Lubrication, Engineering Tribology, (Ed. Butterworth-Heinemann, Burlington, 2006).
- [18] E.d.l.H. M. Flores, D.A. Egidi, R. Ruelas, E. Rodríguez, A. Bautista, P. Corengia., CONAMET SAM 1(2008).
- [19] A. Wennerberg, C. Hallgren, C. Johansson, S. Danelli, Clinical Oral Implants Research **9**, 11(1998).
- [20] E. Maawad, Y. Sano, L. Wagner, H.G. Brokmeier, C. Genzel, Materials Science and Engineering A **536**, 82(2012).
- [21] J.Z. Lu, K.Y. Luo, F.Z. Dai, J.W. Zhong, L.Z. Xu, C.J. Yang, L. Zhang, Q.W. Wang, J.S. Zhong, D.K. Yang, Y.K. Zhang, Materials Science and Engineering A **536**, 57 (2012).
- [22] E. Maawad, H.G. Brokmeier, L. Wagner, Y. Sano, C. Genzel, Surface and Coatings Technology **205**, 3644 (2011).
- [23] S.L.R. da Silva, L.O. Kerber, L. Amaral, C.A. dos Santos, Surface and Coatings Technology **116**, 342 (1999).
- [24] P.C. Peyre, C.; Forget, P.; Beranger, G.; Lemaitre, C.; Stuart, D. Journal of Materials Science **42**, 6866 (2007)
- [25] J.Z. Lu, L. Zhang, A.X. Feng, Y.F. Jiang, G.G. Cheng, Materials & Design **30**, 3673 (2009).
- [26] Y.B. Guo, R. Caslaru, Journal of Materials Processing Technology. **211**, 729 (2011).
- [27] G.M. IL Bengochea, J. Insausti, A. Lucaioli, L. Iurma, CONAMET. **8**, 711 (2003).
- [28] Y. Zhang, J. You, J. Lu, C. Cui, Y. Jiang, X. Ren, Surface and Coatings Technology **204**, 3947(2010).
- [29] R.C. Cozza, J.D.B. de Mello, D.K. Tanaka, R.M. Souza, Wear **263**, 111 (2007).
- [30] R.C. Cozza, D.K. Tanaka, R.M. Souza, Wear **267**, 61 (2009).
- [31] K. Adachi, I.M. Hutchings, Wear **255**, 23 (2003).
- [32] R. Câmara Cozza, Tribology International **57**, 266(2013).
- [33] F.J.G. Silva, R.B. Casais, R.P. Martinho, A.P.M. Baptista, Wear **271**, 2632 (2011).